SSCL-568
LBL-31895

SSCL-568
LBL-31895

Superconducting Super Collider Laboratory

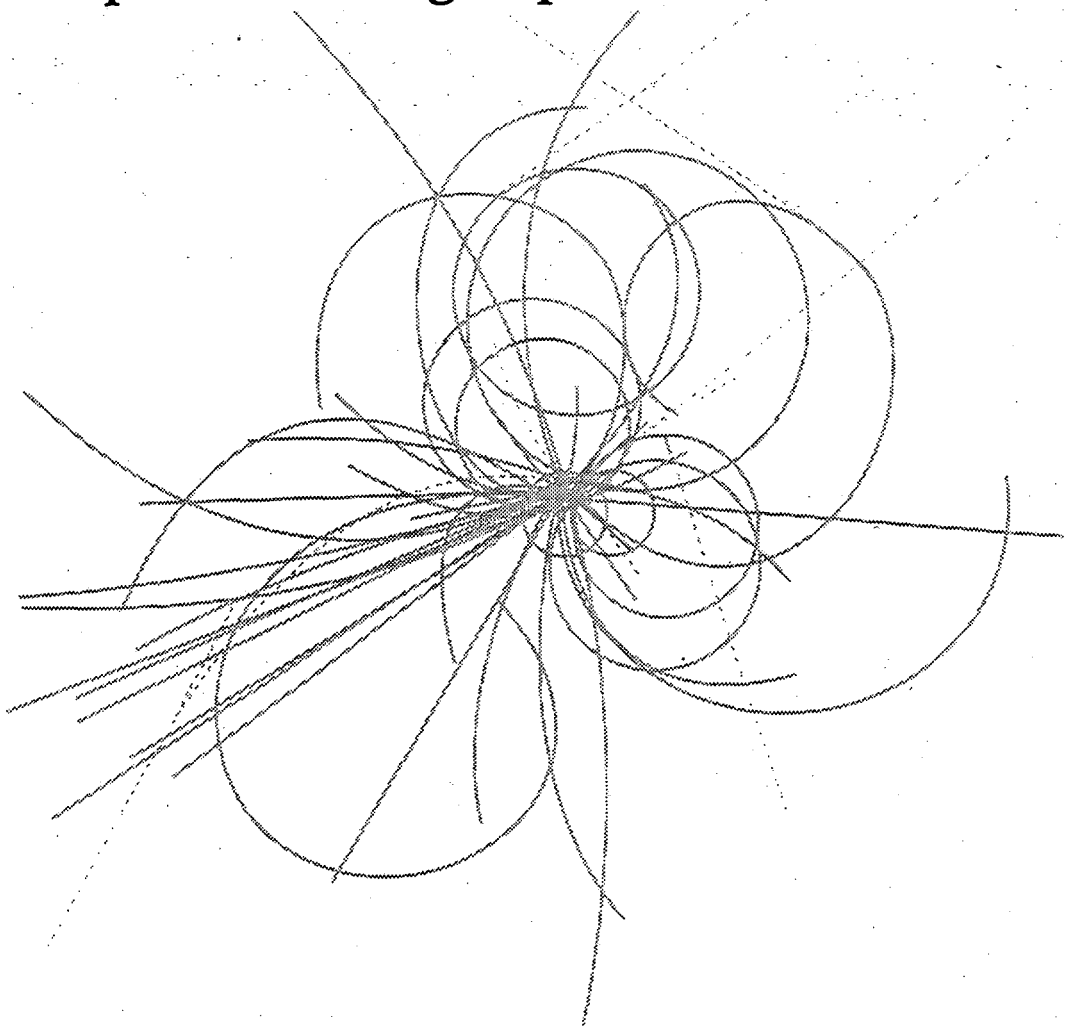

Design of the Main Dipoles and Quadrupoles for the SSC Low Energy Booster

V. Thiagarajan, X. Wu, R. York,
R. D. Schlueter, and K. Halbach

March 1992

DISCLAIMER

SSCL-568
LBL-31895

Design of the Main Dipoles and Quadrupoles for the SSC Low Energy Booster

V. Thiagarajan, X. Wu, R. York

Superconducting Super Collider Laboratory*
2550 Beckleymeade Avenue
Dallas, Texas 75237

and

R. D. Schlueter and K. Halbach

Lawrence Berkeley Laboratory†
1 Cyclotron Road
Berkeley, CA 94720

March 1992

* Operated by the Universities Research Association, Inc., for the U.S. Department of Energy under Contract No. DE-AC35-89ER40486.

† This work supported by the U.S. Department of Energy under contract No. DE-AC03-76SF00098.

SSCL-568
LBL-31895

Design of the Main Dipoles and Quadrupoles for the SSC Low Energy Booster

V. Thiagarajan, X. Wu, R. York, R. D. Schlueter, K. Halbach

Abstract

The SSC Low Energy Booster (LEB) is a synchrotron which accelerates bunches of protons from a momentum of 1.2 Gev/c at injection to a momentum of 12.0 Gev/c at extraction. The main bending dipoles with a peak field of 1.3 Tesla and the main focusing and defocusing quadrupoles with a peak gradient of about 14.9 Tesla/m operate on the same power supply which ramps up sinusoidally from a current of 10% of the peak value at injection to the peak at extraction in a 10 Hz cycle. The ratio of the quadrupole gradient to the dipole strength is kept sufficiently constant over the ramping cycle so as to avoid a tune shift. The magnets are also designed to achieve a prescribed field quality so as to minimize emittance growth during acceleration. This report describes the design of the LEB dipoles and quadrupoles.

1.0 INTRODUCTION

The Low Energy Booster (LEB) receives bunches of protons at a momentum of 1.2 Gev/c from the Linear Accelerator (Linac) and accelerates them to a momentum of 12.0 Gev/c before they are injected into the Medium Energy Booster (MEB). This report describes the physical design of the main dipoles which provide the bending field and the main quadrupoles used in focusing/defocusing. The electrical power supply provides current varying from 10% of the peak value at injection to the peak at extraction in a cycle of 10 Hz. The power supply is a major cost component. Power supply cost increases with the energy stored in the magnet, which in turn increases linearly with the pole width. Hence, there is a compromise between designing to meet the stringent field specifications detailed in the following sections and keeping the pole width as small as possible to minimize power supply costs. Furthermore, the dipoles and the quadrupoles are also required to track during the acceleration cycle, *i.e.*, the ratio of the field gradient of the quadrupole to the bending field of the dipole should be maintained sufficiently constant. Thus, all dipoles and quadrupoles operate on the same power supply, and pole losses are matched over the entire ramping cycle. Additionally, there will be eddy currents induced during the ramping cycle; their effect in the "good field region" is minimized by the magnet design.

The following sections detail the design approach, highlighting useful results from magnet theory and reworking the flexible design specifications as necessary to converge on magnet designs featuring high field quality, good dipole-quadrupole tracking, and minimum cost.

2.0 MAGNETOSTATICS BASICS

The LEB magnets will operate in iron-dominated, resistive regimes. In the current-free region inside the beam tube, fields can be described by Maxwell's equations as follows:

$$\nabla \times E = -\frac{\partial B}{\partial t} \Longrightarrow \nabla \cdot B = 0, \qquad \nabla \times H = 0 \tag{1}$$

where $B = \mu_0 H$. H (and thus B) can be expressed as the gradient of a scalar potential V or, alternatively as the curl of a vector potential A:

$$\mu_0 H = -\nabla V, \qquad B = \nabla \times A. \tag{2}$$

Away from magnet ends fields are two dimensional; A and V satisfy the Cauchy-Riemann equations $A'_x = V'_y$ and $V'_x = -A'_y$, and can thus be represented as the real and imaginary parts of an analytic function F of the complex variable $z = x + iy$:

$$F \equiv A + iV. \tag{3}$$

It follows directly from Eqs. (2) and (3) that the complex conjugate $B^*(z)$ of the field is analytic in z and is given by:

$$B^*(z) = i\frac{dF}{dz}. \tag{4}$$

It is convenient to expand the complex potential F in a power series about a point (say $z = 0$) and analyze the "harmonic" components:

$$F(z) = \sum_{n=1}^{\infty} \left(\frac{z}{r_p}\right)^n c_n; \qquad B^*(z) = i\sum_{n=1}^{\infty} \left(\frac{z}{r_p}\right)^{n-1} \frac{nc_n}{r_p} \tag{5}$$

where r_p is the magnet aperture radius ($\longrightarrow$ half gap h for a dipole). For magnets exhibiting midplane symmetry, the coefficients $c_n \equiv a_n + ib_n$ are pure real (or pure imaginary if A, rather than V, is constant along the midplane). For symmetric multipole magnets (*i.e.*, rotatable by $360°/2m$ with a change of polarity), of order m (*e.g.*, $m = 1$ for dipole, 2 for quadrupole, etc.) the complex potential F and flux density $B^*(z)$ are

$$F(z) = \sum_{n=1}^{\infty} \left(\frac{z}{r_p}\right)^{m(2n-1)} a_{m(2n-1)}; \tag{6a}$$

$$B^*(z) = i\sum_{n=1}^{\infty} \left(\frac{z}{r_p}\right)^{m(2n-1)-1} \frac{m(2n-1)a_{m(2n-1)}}{r_p}. \tag{6b}$$

3.0 INITIAL MAGNET DESIGN

3.1 Initial Magnet Specifications

The magnet excitation current varies from 10% of peak value up to the peak value in a 10 Hz cycle:

$$I = I_{\max}(0.55 + 0.45\sin\phi) \tag{7}$$

where, the phase angle ϕ (deg) is related to time t (sec) by $t = 0.025\left(1.0 + \frac{\phi}{90.0}\right)$.

The dipole excitation is to produce a field strength that cycles between 0.13 Tesla and 1.3 Tesla. The strawman field quality specification for the LEB dipole magnets is that

$$\left|\left(\frac{\Delta B}{B}\right)_d\right| \leq 10^{-4}, \qquad |z| \leq 2.5 \text{ cm}. \tag{8}$$

The gap $2h$ between the dipole pole pieces is to be 5.72 cm in order to accommodate an elliptical beam pipe of approximate dimensions 7.3 cm $\times$ 5.5 cm.

The quadrupole excitation is to produce a field strength that cycles between ~ 1.5 and ~ 15 T/m. Since the quadrupole and dipole are powered together, the exact quadrupole field strength will be determined by the quadrupole/dipole coil turns ratio and the current required to meet the dipole extraction field strength, together with the magnet apertures. The strawman field quality specification for the LEB quadrupole magnets is that

$$\left|\left(\frac{\Delta B}{B}\right)_q\right| \leq 10^{-3}, \qquad |z| \leq 2.0 \text{ cm}. \tag{9}$$

The quadrupole aperture r_p is to be 5.0 cm so as to accommodate the beam pipe.

The strawman tracking specification is that

$$\left|\frac{\Delta(B'_q/B_d)}{B'_q/B_d}\right|_{z=0} \leq 10^{-3} \tag{10}$$

over the entire range of operation, injection to extraction.

These initial specifications are iteratively changed until emittance growth characteristics computed with particle tracking codes fall within acceptable ranges.

3.2 Theoretical Background

3.2.1 High Magnetic Efficiency Baseline Designs

Around the contour comprising the boundaries of Figure 1 or Figure 2, Ampere's Law gives for N turns of a coil carrying I amps:

$$NI = \int_{\text{iron}} H \cdot ds + \int_{\text{air}} H \cdot ds. \tag{11}$$

We define the magnetic efficiency η_{mag} as the ratio of the ampere turns required to attain a given field between the pole pieces to that required in the ideal case where the pole pieces are infinitely permeable, *i.e.*, the magnetic efficiency is that fraction of the excitation current not used to overcome reluctance in the iron:

$$\eta_{\text{mag}} \equiv 1 - \frac{\int_{\text{iron}} H \cdot ds}{NI} = \frac{V_p}{\mu_0 NI} \tag{12}$$

where V_p is the scalar potential at the pole face tip.

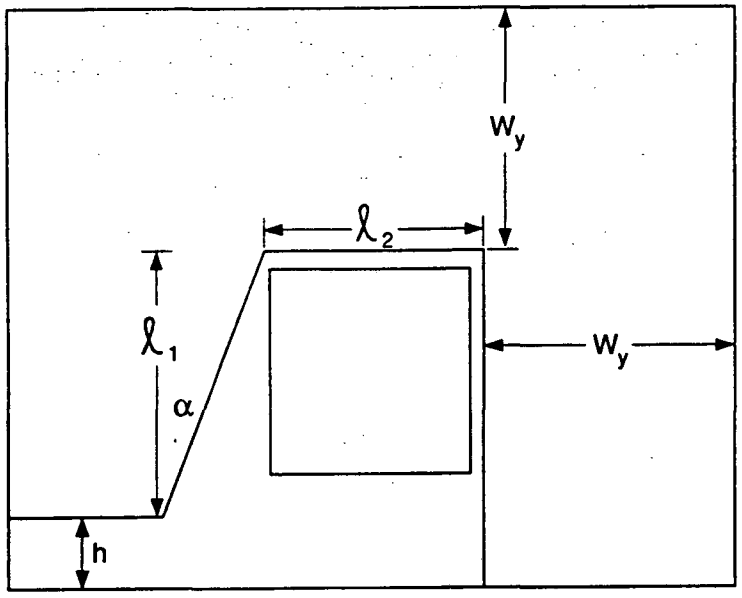

Figure 1. Strawman LEB Dipole Design.

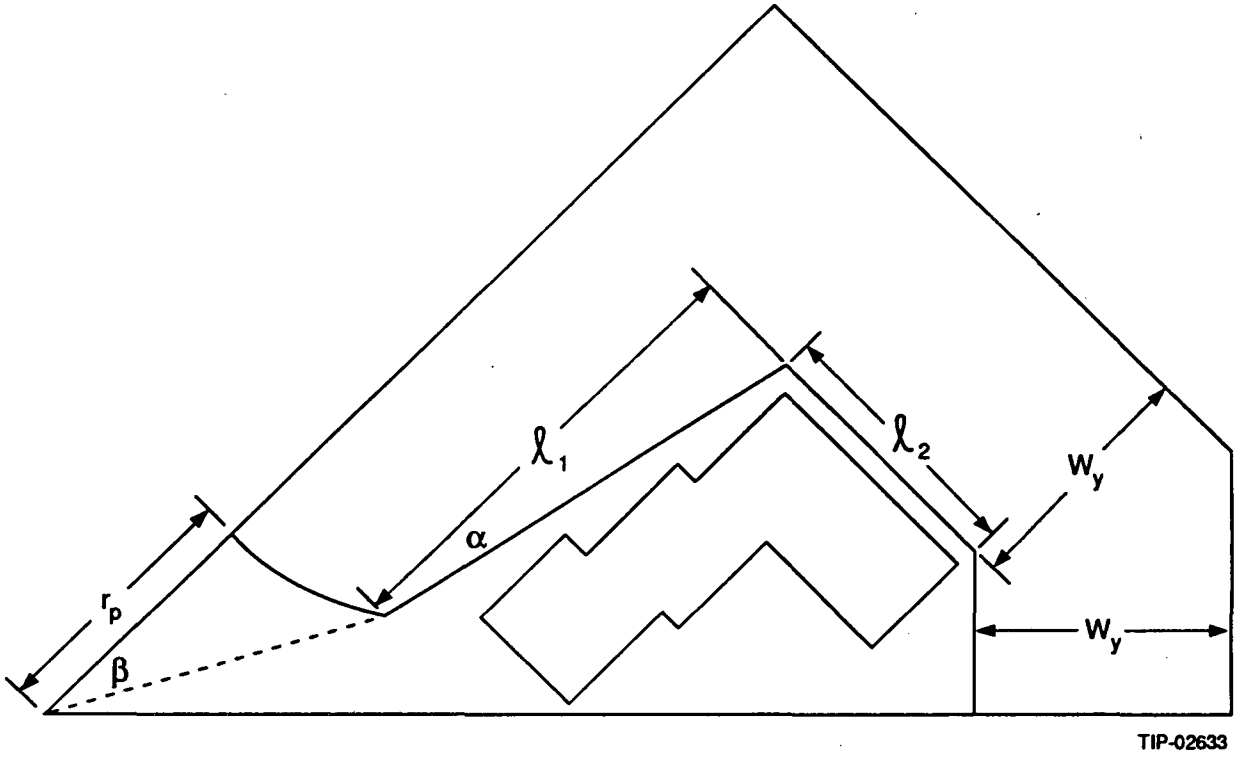

Figure 2. Strawman LEB Quadrupole Design.

At the pole face tip, $\left(\frac{z}{r_p}\right)^m = i$; thus from Eq. (6), $V_p = \sum_{n=1}^{\infty}(-1)^{n-1}a_{m(2n-1)}$ and we have

$$\eta_{\text{mag}} = \frac{\sum_{n=1}^{\infty}(-1)^{n-1}a_{m(2n-1)}}{\mu_0 NI}. \tag{13}$$

It is desirable to keep η_{mag} as near to 100% as is reasonably achievable for several reasons: (1) magnet saturation magnifies any effect that pole-to-pole or lamination-to-lamination nonuniformities have on the fields, (2) magnet saturation implies a greater variation of η_{mag} itself over the excitation ramping cycle, and thus has a deleterious effect on the dipole/quadrupole tracking, and (3) larger variations in the level of pole tip saturation over the ramping cycle worsen the attainable field quality for a given magnet at low and/or high field levels.

Attainable field quality depends primarily on: (1) the saturation of the pole pieces and (2) their physical extent. Degradation of field quality due to the transverse plane truncation of pole tips can be compensated to a large degree by shimming. The attainable field quality that can be expected from a real magnet with such a truncated, shimmed pole tip is given by[1]

$$\left.\frac{\Delta B}{B}\right|_{|z|\leq f^m r_p} \simeq e^{[-7.14(\frac{d}{r_p}+0.25)]} \tag{14}$$

where, as shown in Figure 3(b), in dipole geometry d is the pole overhang beyond the horizontal extent of the specified good field region, r_p is the magnet aperture radius, and f^m describes the extent of the good field region. The required pole width to achieve a given field quality within a specified good field region for any order multipole magnet can be estimated by first making the transformation from the laboratory z-plane, Figure 3(a), to the dipole w-plane, Figure 3(b): $w = z^m/r_p^{m-1}$.

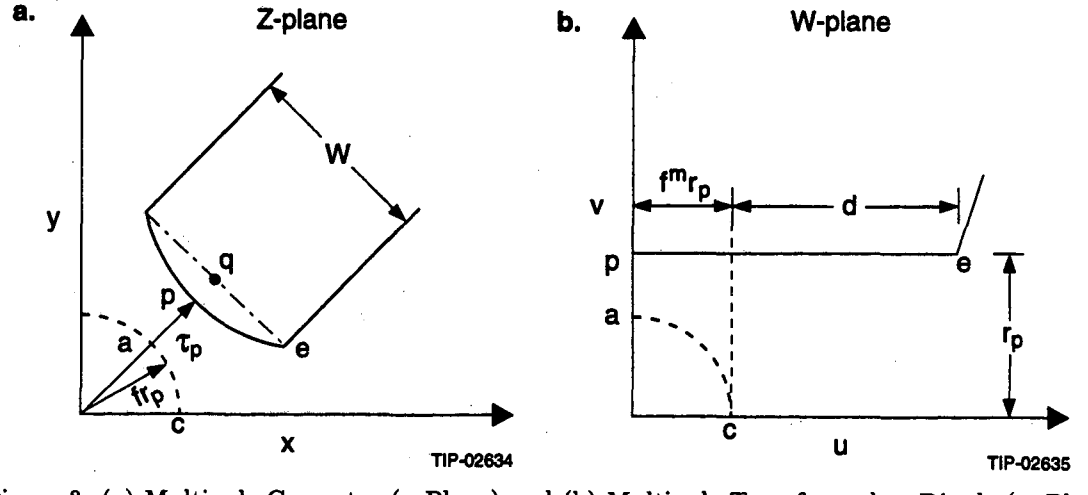

Figure 3. (a) Multipole Geometry (x-Plane) and (b) Multipole Transformed to Dipole (w-Plane).

3.2.2 Dipole-Quadrupole Tracking

For the beam optics, only the first term in Eq. (13) is of importance. Thus, it is convenient to introduce the optical efficiency $\eta_{\rm opt}$ defined by:

$$\eta_{\rm opt} = \frac{a_m}{\mu_0 N I}. \tag{15}$$

Using the expression from Eq. (15) in Eq. (6b) gives for the on-axis dipole field and quadrupole field gradient:

$$B_d^*|_{z=0} = i\frac{a_1}{h} = i\frac{\mu_0 N_d I \eta_{\rm opt_d}}{h}, \qquad \left.\frac{dB_q^*(z)}{dz}\right|_{z=0} = i\frac{2a_2}{r_p^2} = i\frac{2\mu_0 N_q I \eta_{\rm opt_q}}{r_p^2} \tag{16}$$

where the current per coil turn I is common to both the dipole and quadrupole.

The ratio B_q'/B_d on-axis

$$\left.\frac{B_q'}{B_d}\right|_{z=0} = \frac{h}{r_p^2}\frac{2a_2}{a_1} = \frac{h}{r_p^2}\frac{2N_q}{N_d}\frac{\eta_{\rm opt_q}}{\eta_{\rm opt_d}} \tag{17}$$

is to be maintained constant to within the tracking specification given by Eq. (10) during the excitation ramping cycle, otherwise a betatron tuneshift is introduced in the LEB. This necessitates having

$$\left|\frac{\Delta\left(\eta_{\rm opt_q}/\eta_{\rm opt_d}\right)}{\eta_{\rm opt_q}/\eta_{\rm opt_d}}\right| \leq 10^{-3} \tag{18}$$

over the entire excitation ramping cycle. As $(1-\eta_{\rm opt}) \longrightarrow 0$ for both magnets, tracking becomes perfect automatically. If the $\eta_{\rm opt}$'s deviate sufficiently from unity, we have from Eq. (12):

$$\frac{V_{p,q}/N_q}{V_{p,d}/N_d} = \frac{1-\left(\int_{{\rm iron},q} H_q \cdot ds_q/N_q I\right)}{1-\left(\int_{{\rm iron},d} H_d \cdot ds_d/N_d I\right)} \simeq \frac{1-\left(\frac{H_q(I)}{I}\frac{L_q}{N_q}\right)}{1-\left(\frac{H_d(I)}{I}\frac{L_d}{N_d}\right)} \tag{19}$$

where, for the last equality, we assume that iron losses are dominated by H in the region of largest B spanning an extent L in the iron. This ratio is exactly constant only if $\frac{H_q(I)}{I} = \frac{H_d(I)}{I}$ and therefore only if $\frac{L_q}{N_q} = \frac{L_d}{N_d}$, *i.e.*, if the magnitudes of the dominant field regions in the dipole and quadrupole are identical and their lengths scale as the number of turns in their respective coils.

In general, for $V_{p,q}/V_{p,d}$ to be exactly constant, we must have:

$$\frac{\int_{\text{iron},q} H_q \cdot ds_q}{N_q} = \frac{\int_{\text{iron},d} H_d \cdot ds_d}{N_d}. \tag{20}$$

Furthermore, if the iron is significantly anisotropic, the direction of the dominant $B^*(z)$ in the dipole and quadrupole iron should be the same relative to their respective rolling directions.

3.3 Design Approach

The LEB dipole and quadrupole design procedure is structured around three sequential objectives:

1. obtain high magnetic efficiency baseline designs (*i.e.*, as close to 100% as "reasonably" achievable),
2. modify baseline designs to make dipole and quadrupole magnetic efficiencies track, assuming harmonics present can be sufficiently nulled subsequently, and
3. modify dipole and quadrupole pole tips to null harmonics within specified "good field regions."

The magnets are designed using the codes *Poisson*[2] and *Mirt*[2,3]. The code *PE2D*[4] is used to check the results and also to make eddy current calculations. The lamination material is silicon steel (grade M27), modeled with B-H characteristic #3 of Appendix B.

The dipole is designed to have the narrowest possible width amenable to the preceding objectives, which facilitate meeting the specifications listed previously. Stored energy, and hence, the cost of electrical components, is thus minimized.

The dipole and quadrupole magnets operate on the same electrical bus; their fields are related by Eq. (17). For a maximum dipole field of 1.3 T, half gap $h = 2.86$ cm, quadrupole aperture $r_p = 5.0$ cm, and for ideal magnets (*i.e.*, infinitely permeable poles of infinite extent), setting the quadrupole/dipole coil turns ratio $N_q/N_d = 1/2$ results in an acceptable maximum quadrupole gradient of 14.87 T/m.

The choice of N_q and N_d is dictated by engineering concerns such as coil winding, overhang, etc. Chosen turns are $N_q = 4$ and $N_d = 8$.

The excitation coil current densities are $J_{\text{rms}} \approx 4.0$ amp/mm^2 for the dipole and $J_{\text{rms}} \approx 5.0$ amp/mm^2 for the quadrupole. They are chosen as a compromise between minimizing capital and operating costs.[5]

The initial magnet design following the preceding sequence is detailed in Appendix A, where design choices for dipole half-gap, half-width, conductor/insulator package size

and axial curvature along with quadrupole aperture radius, tip corner angle β, conductor/insulator package size, and taper angle α are discussed. Also discussed in Appendix A are design choices affecting dipole-quadrupole tracking, including the quadrupole design featuring a hole to bolt laminations together, and design choices affecting dipole and quadrupole field quality.

4.0 FINAL MAGNET DESIGNS

4.1 Dipole and Quadrupole Magnet Final Designs

As the design is finalized, the dipole coil shape is slightly modified; the final total conductor/insulator package size of $\Delta x \times \Delta y = 7.45 \times 9.25$ cm is chosen. It is found convenient from an engineering point of view to have eight pairs of conductors, each pair carrying the same current (in parallel) as does a single conductor in the quadrupole. The conductors are paired such that one member of each pair lies above the magnet midplane while the other member lies at the conjugate location below the midplane. Such a pairing insures that the current in the two conductors is identical; no flux passes between the two conductors so arranged. Individual conductors are 21 mm $\times$ 18 mm with a 9.0-mm hole in the center for the water passage. The rms current density in the dipole is approximately 4.0 amp/mm^2.

For construction ease, the staggered quadrupole coil design of Figure 2 is replaced in the final design with an "L" shaped coil arrangement. Quadrupole lamination dimensions are modified slightly to accommodate the new coil profile, while maintaining tracking performance.

Field distributions and harmonics from *Poisson*[2] are used for particle tracking using the code *Dimad*.[6] Particles with different normalized emittance ϵ_N are tracked for 1000 turns and the relative emittance variation $\frac{\Delta\epsilon}{\epsilon} = \frac{\epsilon_{max}-\epsilon_{min}}{\epsilon_{average}}$ is calculated. Quadrupole and sextupole systematic errors are included in the tracking. The emittance growth for a dipole with a half-pole width of 6.0 cm is compared with expected characteristics for a perfect machine in Figure 4(a,b,c,d) for both horizontal and vertical planes at extraction and injection; it is far above tolerable limits so the field quality specification for the LEB dipole magnets is revised:

$$\left|\left(\frac{\Delta B}{B}\right)_d\right| \leq 10^{-4}, \qquad |z| \leq 1.40 \text{ cm at extraction},$$
$$|z| \leq 3.25\cos\theta + i2.5\sin\theta \text{ cm at injection.} \qquad (21)$$

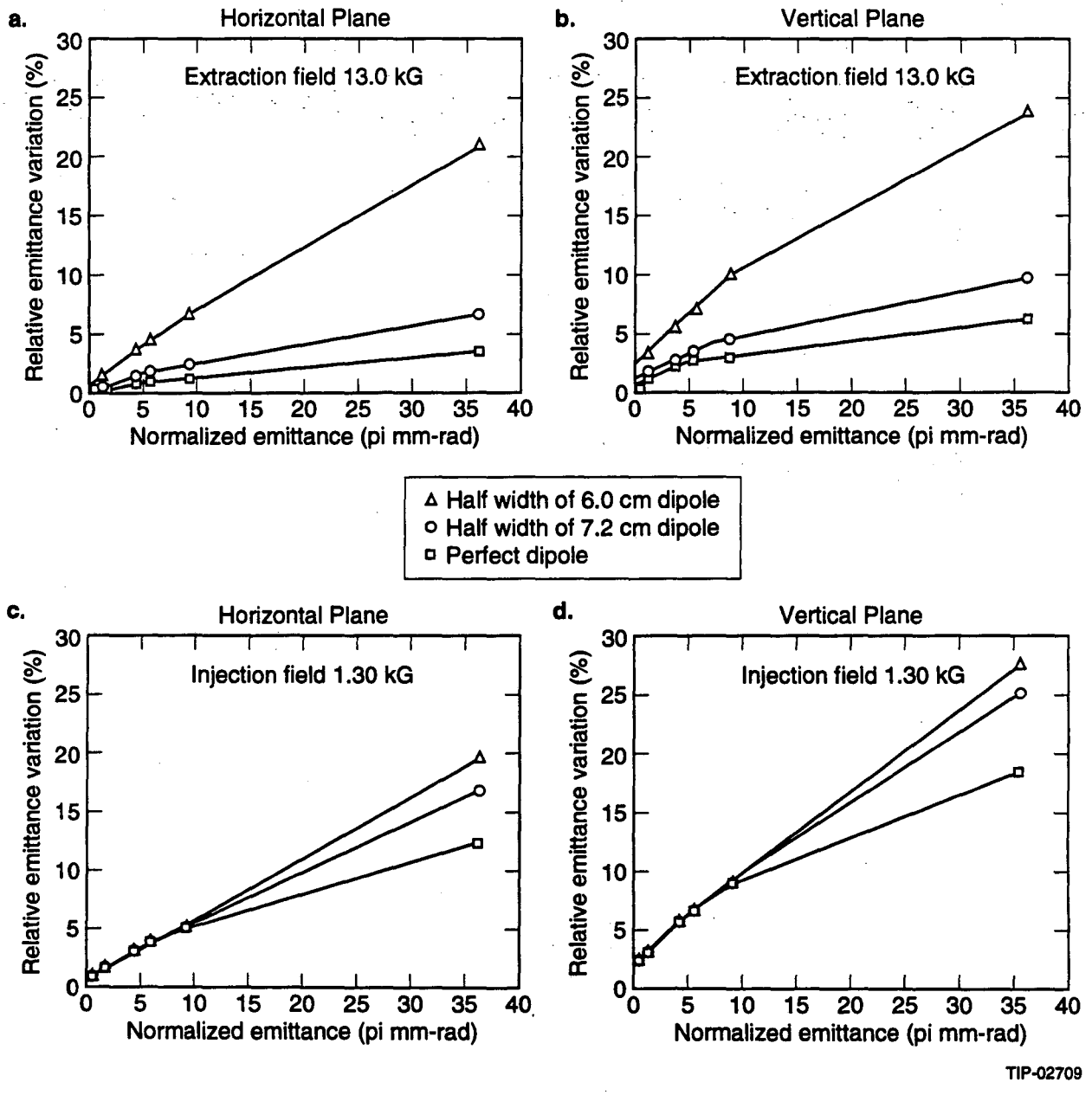

Figure 4. Emittance Growth for Candidate Dipole Final Designs.

Similarly, the field quality specification for the LEB quadrupole magnets is revised:

$$\left|\left(\frac{\Delta B}{B}\right)_d\right| \leq 10^{-3}, \qquad \begin{array}{l} |z| \leq 4.0 \text{ cm at extraction,} \\ |z| \leq 4.25 \text{ cm at injection.} \end{array} \tag{22}$$

Pole shimming is accomplished using *Mirt*[2,3] to simultaneously optimize the tip shape for both high field ($B = 1.3$ T) within the region $|z| \leq 1.40$ cm and low field ($\mu_r = \infty$) within the region $|z| \leq 3.25\cos\theta + i2.5\sin\theta$ cm.

Field quality and emittance growth for candidate final dipole designs of various half-widths (and correspondingly appropriate yoke widths) are shown in Table 1, part 1a and Figure 4, respectively.

TABLE 1. Field Quality for Candidate Final Dipole Designs.

	Run #	Nom. Pole Width (cm)	$\lvert\Delta B/B\rvert_{\text{ext}}$ $\lvert z\rvert \leq 1.40$ cm	$\lvert\Delta B/B\rvert_{\text{inj}}$ $\lvert z\rvert \leq 3.25\cos\theta + i2.5\sin\theta$ cm
1a	D26kct	6.75	0.000134	0.000153
	D26u	6.90	0.000116	0.000082
	D26v	7.05	0.000104	0.000043
	D26vm2	7.20	0.000075	0.000011
1b	D26vm2as	7.20	0.000035	0.000033
			$\lvert\Delta B/B\rvert_{\text{ext}}$ $\lvert z\rvert \leq 4.0$ cm	$\lvert\Delta B/B\rvert_{\text{inj}}$ $\lvert z\rvert \leq 4.0$ cm
1c	Q28g1smr	$\beta = 28°$	0.00078	0.00045

Finally, the coordinates of the *Mirt*ed dipole lamination D26vm2 are rounded to a hundredth of a millimeter and pole tip corners are smoothed. The final dipole design D26vm2asb (Table 1, part 1b) features a shimmed pole tip with a nominal pole half-width of 7.2 cm; further improvement in field quality is deemed not worth the increased energy cost associated with wider poles. Shimmed dipole D26vm2asb injection field quality is $|\Delta B/B| \simeq 0.000035$ at $|z| \leq 3.25\cos\theta + i2.5\sin\theta$ cm; extraction field quality is $|\Delta B/B| \simeq 0.000033$ at $|z| = 1.40$ cm. Figure 5 shows a schematic diagram of the final dipole design D26vm2asb and Table 2 lists the harmonic coefficients at $z = r_p$ from *Poisson*,[2] *i.e.*, the $\frac{(2n-1)\,a_{(2n-1)}}{r_p}$ portion of Eq. (6b).

The final quadrupole design Q28g1smra differs from the strawman Q28g1s in its "L" shaped coil profile and thus slightly enlarged lamination dimensions, the addition of notches

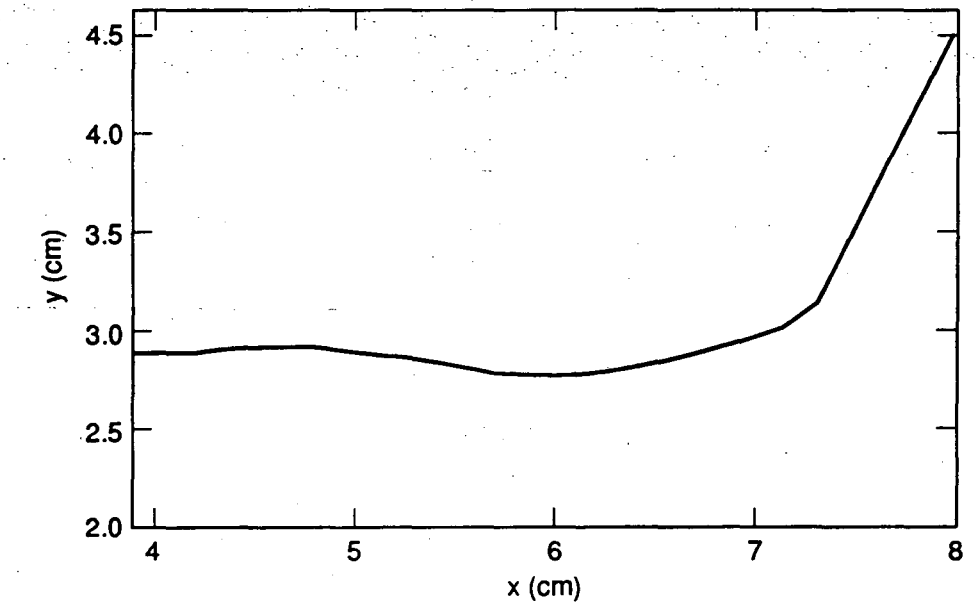

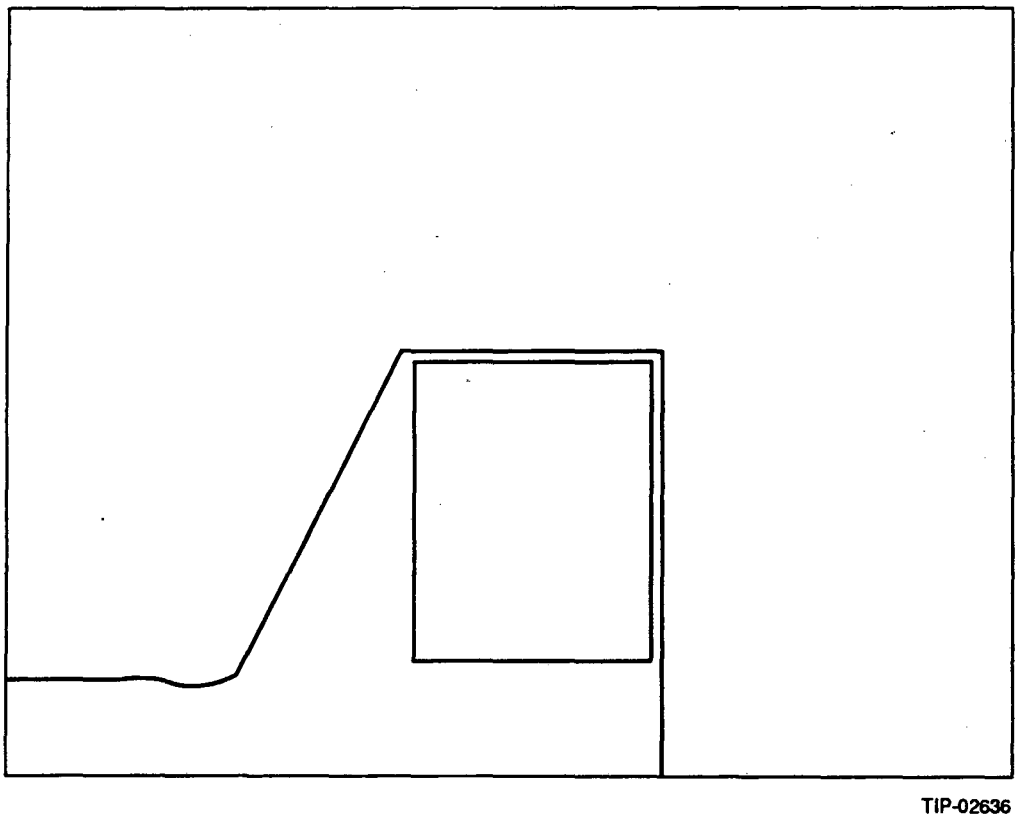

TIP-02636

Figure 5. Schematic of Final Dipole Design.

TABLE 2. Harmonic Coefficients of Final Dipole Design.

$2n-1$	$f \equiv I/I_{\rm ext}$					
	0.10	0.50	0.80	0.90	1.00	1.10
	$\frac{(2n-1)\,a_{(2n-1)}}{r_p}$					
1	−3.7565 E+3	−1.8827 E+4	−3.0043 E+4	−3.3716 E+4	−3.7278 E+4	−4.0527 E+4
3	2.1540 E−2	1.1676 E−1	5.9946 E−1	1.3322 E+0	3.3564 E+0	7.6953 E+0
5	1.0593 E−3	3.5537 E−3	5.3578 E−2	1.9436 E−1	6.2080 E−1	1.3832 E+0
7	−2.1465 E−3	−8.2280 E−3	−6.0818 E−3	1.1448 E−2	6.1891 E−2	1.1448 E−1
9	−5.8526 E−5	9.3641 E−4	2.3410 E−3	9.3641 E−4	1.4046 E−3	1.8728 E−3
11	3.5234 E−3	1.4093 E−2	2.5123 E−2	2.2672 E−2	3.4314 E−2	4.5344 E−3
13	2.2053 E−3	8.8213 E−3	9.6233 E−3	1.3633 E−2	2.7266 E−2	1.7643 E−2
15	7.8714 E−4	2.0990 E−3	4.1981 E−3	−1.4693 E−2	1.6792 E−2	−1.4693 E−2
current excitation at extraction: $mI_{\rm ext}/31\,000 = 0.973103$						

for fiducialization, a slightly thicker upper back leg to compensate for the other changes and thus maintain tracking performance, and the rounding of the *Mirt*ed lamination coordinates to a hundredth of a millimeter. Quadrupole Q28g1smra (Table 1, part 1c) injection field quality is $|\Delta B/B| \simeq 0.0005$ at $|z| \leq 4.0$ cm; extraction field quality is $|\Delta B/B| \simeq 0.0008$ at $|z| = 4.0$ cm. Figure 6 shows a schematic of the final quadrupole design and Table 3 lists the harmonic coefficients at $z = r_p$ from *Poisson*[2], *i.e.*, the $\frac{2(2n-1)a_{2(2n-1)}}{r_p}$ portion of Eq. (6b).

TABLE 3. Harmonic Coefficients of Final Quadrupole Design.

$2(2n-1)$	$f \equiv I/I_{\rm ext}$					
	0.10	0.50	0.80	0.90	1.00	1.10
	$\frac{2(2n-1)\,a_{2(2n-1)}}{r_p}$					
2	−1.8790 E+3	−9.4213 E+3	−1.5037 E+4	−1.6868 E+4	−1.8608 E+4	−2.0178 E+4
6	−1.1351 E+0	−5.7435 E+0	−8.6546 E+0	−8.6427 E+0	−7.2662 E+0	−4.0909 E+0
10	1.4273 E+0	7.1600 E+0	1.1514 E+1	1.3219 E+1	1.5240 E+1	1.7628 E+1
14	1.6072 E+0	8.0761 E+0	1.2863 E+1	1.4358 E+1	1.5741 E+1	1.6821 E+1
Current excitation at extraction: $mI_{\rm ext}/31\,000 = 0.973103$						

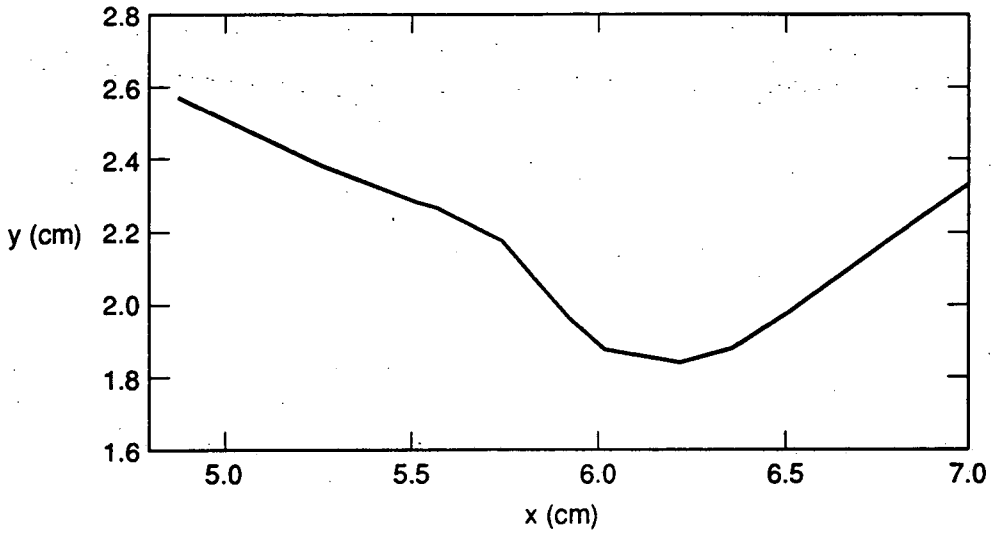

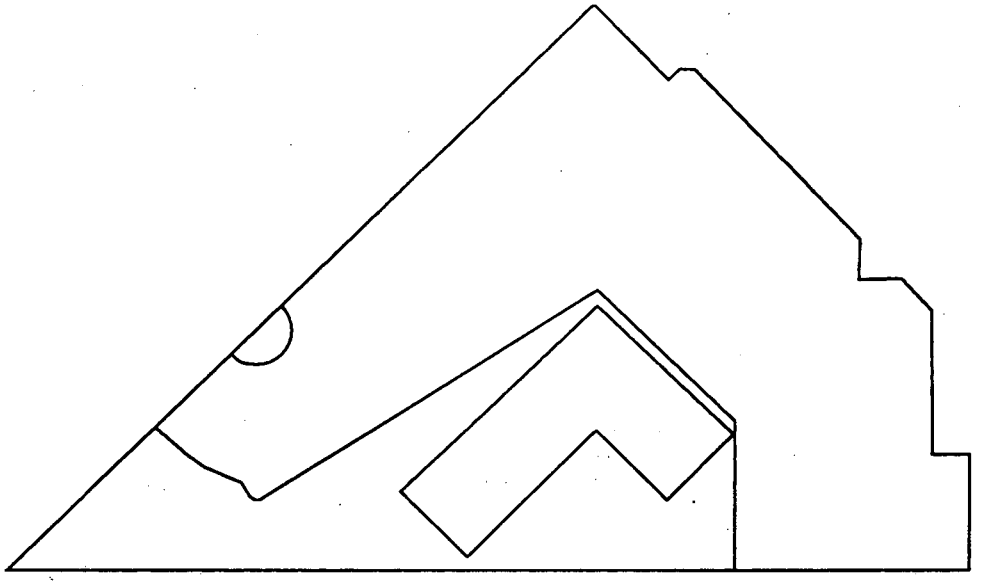

TIP-02637

Figure 6. Schematic of Final Quadrupole Design.

Final dipole and quadrupole designs, D26vm2asb and Q28g1smra track to within 0.0020 over the range from injection to extraction, as shown in Table 4.

TABLE 4. Tracking of Shimmed Final Dipole-Quadrupole Design Pair.

Run (#)	α (deg)	w_y (cm)	$\frac{mI_{ext}}{31\,000}$	$f \equiv I/I_{ext}$ 0.10	0.50	0.80	0.85	0.90	0.95	1.00	1.10
				η_{mag}							
D26vm2asb	25.6	11.10	0.973224	0.9910	0.9933	0.9909	0.9898	0.9881	0.9853	0.9835	0.9676
Q28g1smra	12.0	5.4	0.973103	0.9905	0.9933	0.9907	0.9896	0.9882	0.9863	0.9812	0.9721
				η_{opt}							
D26vm2asb	25.6	11.10	0.973224	0.9910	0.9933	0.9907	0.9901	0.9882	0.9863	0.9834	0.9719
Q28g1smra	12.0	5.4	0.973103	0.9913	0.9941	0.9917	0.9906	0.9888	0.986	0.9817	0.9678

4.2 Field Quality Sensitivity

Sensitivity to yoke thickness. Increasing the yoke thickness w_y by 1 millimeter has the effect of increasing η_{mag} at extraction by 0.0006; η_{mag} at injection is unaffected. A tolerance of ± 0.167 mm on w_y puts resulting η_{mag} variations an order of magnitude below the tracking specification.

4.3 Magnet Eddy Currents

Magnet thermal losses and stored energies obtained from dynamic *PE2D*[4] runs are recorded in Table 5.

TABLE 5. Thermal Loss, Stored Energy, and Inductance of Final Magnet Designs.

		Dipole			Quadrupole		
Time (sec)	I/I_{max}	Thermal Loss (kW/m)	Stored Energy (J/m)	Inductance (mH/m)	Thermal Loss (kW/m)	Stored Energy (J/m)	Inductance (mH/m)
0.010	0.186	0.78	319	1.295	1.06	125	0.508
0.020	0.411	3.23	1561	1.300	4.38	616	0.513
0.025	0.550	5.10	2802	1.303	6.85	112	0.517
0.030	0.689	7.16	4402	1.304	9.52	1756	0.520
0.040	0.914	10.80	7737	1.303	14.06	3120	0.525
0.050	1.000	12.14	9247	1.303	15.57	3769	0.530

Coil current excitation is given by Eq. (7) with $I_{\max} = 3770.8$ amp/turn. Copper conductivity $\sigma = 0.5882 \cdot 10^8$ S/m.

For the dipole, cross-sectional area per pair of conductors in parallel is 638.8 mm^2; there are eight such pairs per half-plane. Average integrated thermal loss is 5.68 kW/m. Lamination loss (hysteresis, eddy, and anamolous) for the dipole is $\sim$ 658.0 W/m.

For the quadrupole, cross-sectional area per conductor is 498.4 mm^2; there are four such conductors per quadrant. Average integrated thermal loss is 7.46 kW/m. The lamination loss (hysteresis, eddy, and anamolous) for the dipole is $\sim$ 237.0 W/m.

These runs are also compared with field quality results from *Poisson*. The actual design packing factor of 0.97 is used in the *Poisson* runs while a packing factor of 1.0 is used in the *PE2D* runs, thus the field quality obtained with *PE2D* is slightly better than that from *Poisson*.

4.4 Summary

At the time of writing this report, the LEB dipole and quadrupole laminations were undergoing minor engineering changes which do not affect the physical design and tracking. Each quadrant of the dipole has sixteen conductors 18 $\times$ 21 mm^2 with a 9 mm hole for water passage. Each pair of these conductors carries the bus current of 3770.8 amperes (at full excitation for 1.3 Tesla). The quadrupole has four conductors in each octant 23 $\times$ 21.9 mm^2 with a 6.5 mm hole for water passage. The peak field of the dipole will be raised to 1.35 Tesla, and this requires a bus current of 3918.6 amperes. If the field were increased to 1.4 Tesla, the bus current will increase to 4086.8 amperes. The gradient of the quadrupole corresponding to a dipole field and given excitation and corresponding efficiencies is given by Eq. (17). The quality of tracking described by Eq. (18) is 0.0021 at a field of 1.3 Tesla and is 0.0046 at a field of 1.4 Tesla. The quality of tracking is much less than the specified value of 0.001 for fields less than 1.3 Tesla. The current laminations for the dipole and the quadrupole are shown in Figures 7 and 8.

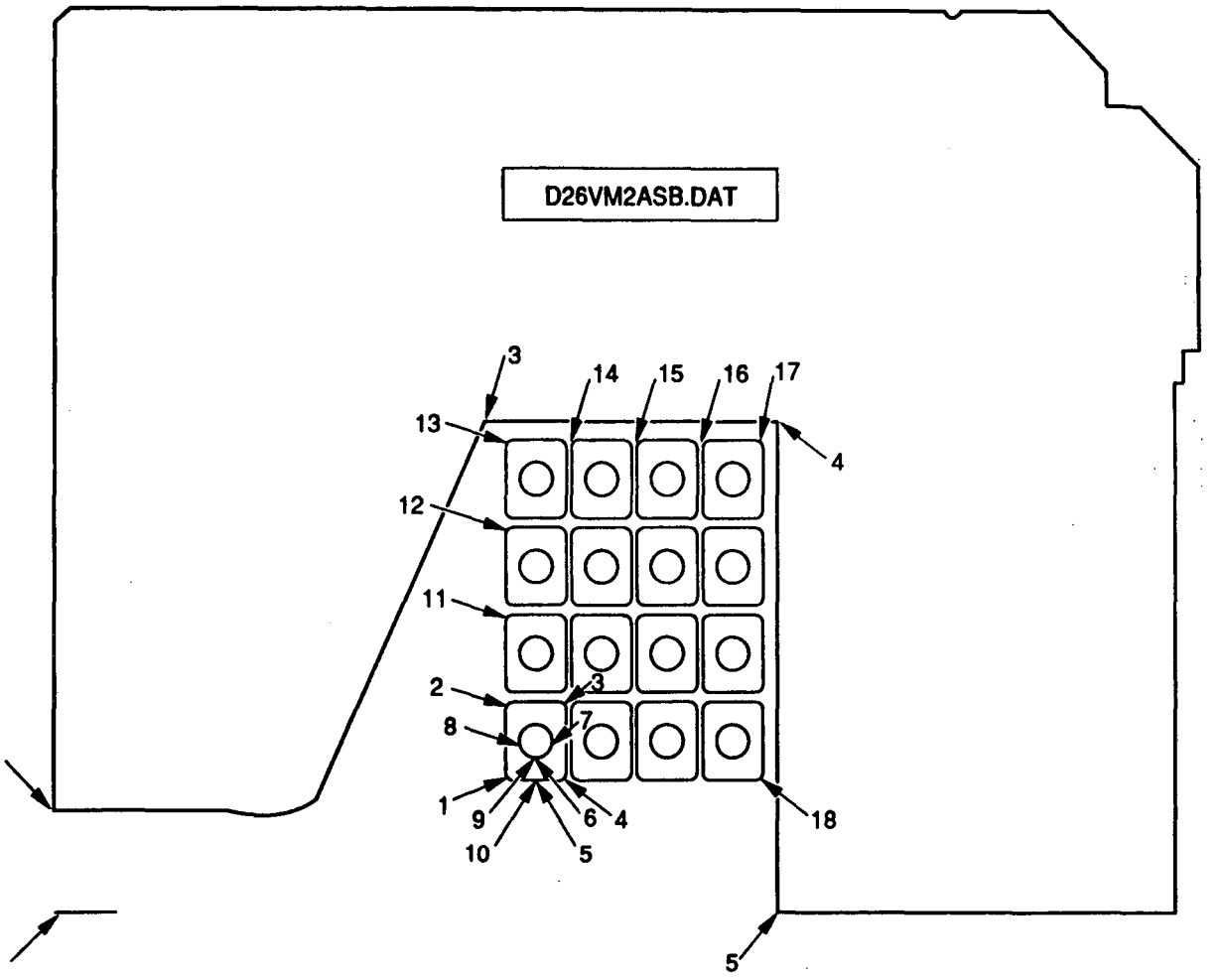

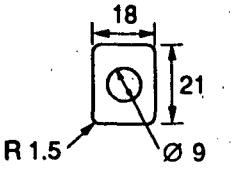

Area = 312.45 mm

Lamination points		
pnt	X0	Y0
1	0.0000	0.0000
2	0.0000	28.6000
3	122.0000	133.0000
4	204.5000	133.0000
5	204.5000	-.0000

Conductor points		
pnt	X0	Y0
1	125.6979	35.4412
2	125.6979	56.4412
3	143.6979	56.4412
4	143.6979	35.4412
5	134.6979	35.4412
6	134.6979	41.4412
7	130.1979	45.9412
8	139.1979	45.9412
9	134.6979	41.4412
10	134.6979	35.4412
11	125.6979	79.7984
12	125.6979	104.5780
13	125.6979	127.9352
14	144.5310	127.9352
15	163.3641	127.9352
16	182.1972	127.9352
17	200.1972	127.9352
18	200.1972	35.4412

TIP-02711

Figure 7. Current Laminations for the LEB Dipole.

Lamination points		
pnt	X0	Y0
1	0.00	0.00
2	35.36	35.36
3	38.00	32.89
4	40.00	31.25
5	42.00	29.76
6	44.00	28.41
7	46.00	27.17
8	48.00	26.04
9	48.65	25.70
10	50.28	24.84
11	51.91	24.01
12	53.61	23.29
13	55.59	22.65
14	57.28	21.74
15	58.72	20.01
16	59.48	19.11
17	60.20	18.68
18	62.19	18.50
19	63.59	18.97
20	64.75	19.88
21	65.81	20.76
22	66.98	21.49
23	144.97	71.21
24	178.39	37.79
25	178.39	0.00
26	242.77	0.00
27	242.77	30.40
28	232.39	30.25
29	232.39	68.65
30	223.65	77.39
31	213.49	77.39
32	213.49	87.55
33	170.82	130.22
34	166.32	130.22
35	164.08	127.98
36	146.03	146.03
37	64.49	64.49
38	64.49	55.51
39	55.51	55.51
40	35.36	35.36

Conductor points		
pnt	X0	Y0
1	95.37	20.07
2	110.86	35.55
3	127.12	19.29
4	111.64	3.80
5	103.51	11.94
6	108.95	17.38
7	113.55	17.38
8	108.95	21.98
9	108.95	17.38
10	103.51	11.94
11	111.99	36.68
12	128.60	53.29
13	144.09	68.78
14	160.94	51.93
15	177.20	35.66
16	161.72	20.18
17	144.86	37.03
18	128.25	20.42

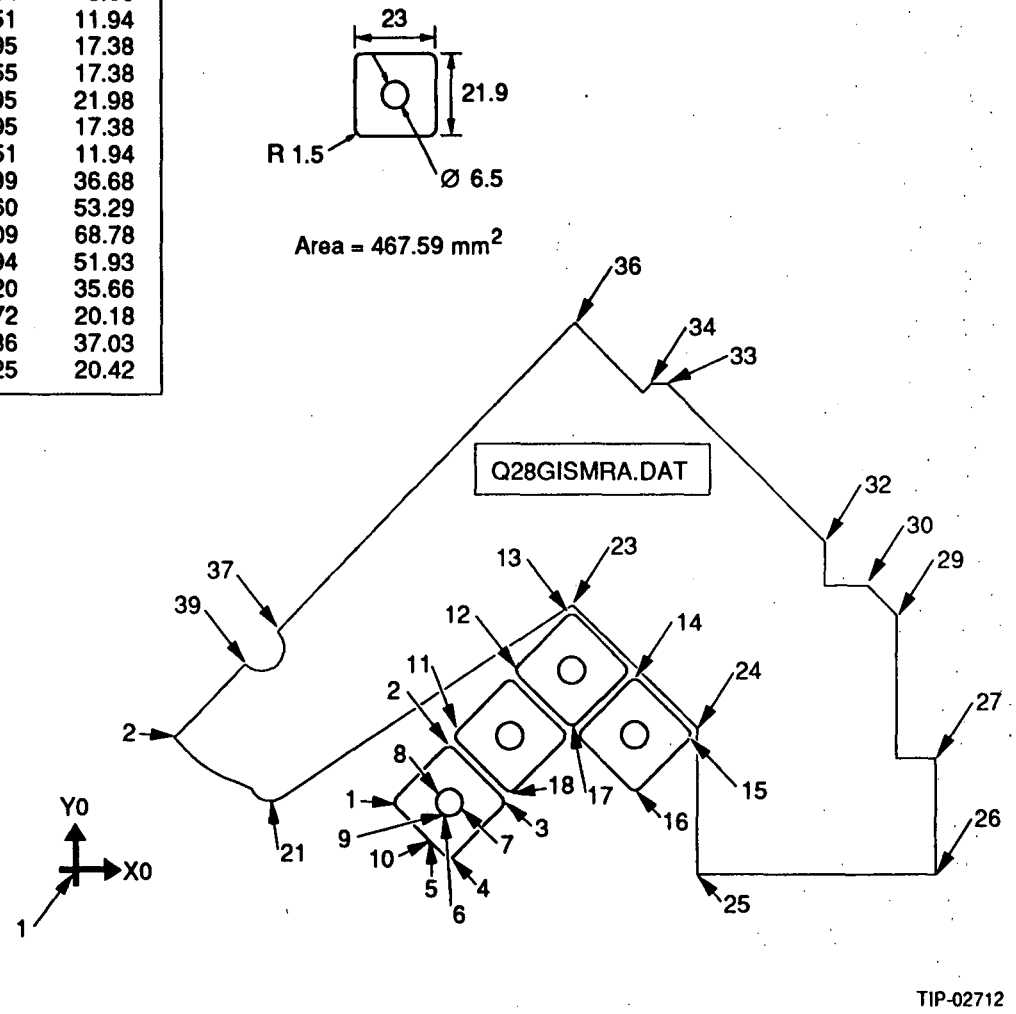

Figure 8. Current Laminations for the LEB Quadrupole.

ACKNOWLEDGEMENTS

The authors thank G.E. Fischer, Roger Zink and Warner Heilbrunn for many helpful insights spanning a wide range of magnet design aspects.

REFERENCES

1. Halbach, K., *Insertion Device Design*, Report No. V-8811-1.1-16, Lawrence Berkeley Laboratory, Berkeley CA, March 1989.
2. *Reference Manual for the Poisson/Superfish Group of Codes*, LA-UR-87-126, Los Alamos National Laboratory, Los Alamos, NM, 1987.
3. Halbach, K., *A Program for Inversion of System Analysis and Its Application to the Design of Magnets*, 2^{nd} Int. Conf. on Magnet Tech., Oxford, July 1967.
4. *PE2D Reference Manual*, Version 8.2, Vector Fields Inc., Aurora, Ill.
5. Fischer, G.E., *Iron Dominated Magnets*, AIP Conf., 153, V2, New York, 1987.
6. Servranckx, R., Brown, K., Schachinger, L., and Douglas, D., *Users Guide to the Program Dimad*, SLAC Report 285 00-28.

APPENDIX A
INITIAL MAGNET DESIGN DETAILS

A.1 HIGH MAGNETIC EFFICIENCY BASELINE DESIGNS

A.1.1 Baseline Dipole Design

Maintaining the dipole quality consists of designing the pole so as to avoid magnetic saturation and shaping the tip so as to compensate for the finite transverse extent of the poles. The chosen half gap $h = 2.86$ cm is large enough to accommodate the beam pipe.

From Eq. (14) a dipole half width of $\sim 2.5 + 1.04h = 5.5$ cm is needed to maintain a field quality of $|\Delta B/B| \leq 0.0001$ for $|z| \leq 2.5$ cm. Strawman LEB dipole design candidates feature a half-pole width $w = 6.0$ cm.

A strawman total conductor/insulator package size of $\Delta x \times \Delta y = 7.85 \times 8.46$ cm is chosen, corresponding to an rms dipole coil current density $\simeq 4.0$ amp/mm^2. The dipole vertical dimensions l_1 and l_2 allow for sufficient coil package clearance in the gap during assembly, see Figure 1 of the basic report. (Subsequently referenced non-prefixed figure numbers are from the basic report).

The effect of dipole taper angle α on extraction (*i.e.*, $B_d = 1.3$ T) magnetic efficiency is tabulated in Table A-1, part 1a. As α increases, η_{mag} increases (given a sufficiently thick yoke), but so does physical dipole size (iron width and height). Design D21b is about as small as the dipole can be while keeping $\eta_{\mathrm{mag}} \geq 98\%$. Table A-1, part 1b shows that for dipole design D21, as yoke thickness w_y decreases below 10 cm; η_{mag} drops sharply. For the alternative dipole design D30 with larger α and with a yoke thickness $w_y = 12$ cm, (Table A-1, part 1c), an extraction $\eta_{\mathrm{mag}} = 0.987$ is attainable. The corresponding injection $\eta_{\mathrm{mag}} = 0.9905$ is marginally sensitive to α insofar as the iron path length increases. Efficiency sensitivity to yoke thickness at injection is negligible. Larger α requires a thicker yoke to realize full magnetic efficiency capability.

If the dipole magnet were straight axially, an additional 3.3 cm pole tip half-width would be required to accommodate the sagitta. Table A-1, part 1d shows that an additional yoke thickness increment of ~ 3.3 cm is necessary to keep η_{mag} from dropping. Thus, for the straight dipole design, a total dipole lamination increment of +13.2 cm on the width and +6.6 cm on the height is required. The additional stored energy due to the 6.6 cm sagitta over the 5.72 cm dipole gap for the ramping 1.3 T field is ~ 2.5 kJ per-meter-length of dipole. We choose to to avoid these huge material and power cost penalties, and thus accept the additional complexity of axially-curved dipoles.

TABLE A-1. Dipole Geometry and Magnetic Efficiency for Strawman Designs.

	Run (#)	α (deg)	w_y (cm)	η_{mag}	$I_{\text{coil}}/31\,000$	Comments
	D11b	10.85	10	0.9624	0.993767	
	D11c	10.85	15	0.9648	0.991377	η_{mag} virtually the same,
	D16b	16.03	10	0.9722	0.981578	$w_y = 10$ cm is sufficient
1a	D16b	16.03	10	0.9722	0.981578	
	D21b	20.96	10	0.9805	0.975210	
	D26b	25.59	10	0.9817	0.973860	
	D30b	29.89	10	0.9777	0.975763	η_{mag} falling, $w_y = 10$ cm is not enough at this larger α
1b	D21d	20.96	9	0.9676	0.987880	η_{mag} falling fast
	D21e	20.96	8	0.9194	1.039208	η_{mag} falling faster
1c	D30f	29.89	12	0.9870	0.967268	
	D30fz	29.89	12	0.9905	0.0967268	at injection, baseline data
1d	D21bs	20.96	10	0.8979	1.062819	η_{mag} drops, need thicker yoke
	D21fs	20.96	13.3	0.9844	0.971169	
$B = 13\,000$ for all cases except D30fz, which is at injection excitation						

A.1.2 Baseline Quadrupole Design

Maintaining the quadrupole quality consists of designing the pole to avoid magnetic saturation and shaping the tip to compensate for the finite transverse extent of the poles. The chosen aperture radius $r_p = 5.0$ cm is large enough to accommodate the beam pipe, yet sufficiently small enough to avoid major saturation problems in the poles at peak excitation.

Let us transform to dipole (w-plane) geometry, $w = z^m/r_p^{m-1}$. To maintain a field quality of $|\Delta B/B| \leq 0.001$ for $|z| \leq 2.0$ cm, we have $d/r_p = 0.717$ from Eq. (14). From Figure 3(b), this requires a dipole-transformed half width of $\sim \left(\frac{2}{r_p}\right)^2 r_p + 0.717 r_p = 4.4$ cm, which corresponds to an angle β of 21° in quadrupole geometry (Figure 2). Strawman LEB quadrupole design candidates feature pole angles of $\beta = 23.0°$ or 28.0°.

A staggered array of four 2.3 × 2.3 cm coil/insulator packages with 6.5 mm diameter holes in the center for water passages is chosen, corresponding to an rms dipole coil current density $\simeq$ 5.0 amp/mm^2. The current is $\sim$ 3700.0 amperes-per-turn. The rms current is 0.635 times the peak current. The quadrupole dimensions l_1 and l_2 in Figure 2 allow for sufficient coil package clearance.

The effect of quadrupole pole angle β and taper angle α on extraction (*i.e.*, B'_q = 14.87 T/m) magnetic efficiency is tabulated in Table A-2, part 2a. The difference in magnetic efficiencies for the two pole angles β at the same taper angle α is slight. The increased pole-to-pole parasitic flux at $\beta = 28°$ is not enough to cause pole magnetic saturation. Thus we choose for our strawman quadrupole $\beta = 28°$ for its superior harmonics rejection capability.

TABLE A-2. Quadrupole Geometry and η_{mag} for Strawman Designs.

			$\beta = 28°$	$\beta = 23°$
	α (deg)	w_y (cm)	η_{mag}	η_{mag}
	4	7	0.964	
	8	7	0.982	
	9.2	7		0.981
2a	12	7	0.988	
	13.0	7		0.989
	16	7	0.990	
	16.6	7		0.991
	20.2	7		0.992
	12	7	0.988	
2b	12	6	0.987	
	12	5	0.984	
	12	4	0.957	

For $\beta = 28°$, I = 15 500 amp and B' varies slightly.
For $\beta = 23°$, B' = 1487 G/cm and I varies slightly.

As α increases, η_{mag} increases, though with diminishing returns due to the increase in parasitic flux. We choose $\alpha = 12°$; the staggered coil package shown in Figure 2 can still

be accommodated with this geometry. Table A-2, part 2b shows that for the quadrupole design with $\beta = 28°$ and $\alpha = 12°$, a quadrupole yoke thickness $w_y = 5$ cm is sufficient to avoid significant pole saturation. As with the dipole, quadrupole $\eta_{\rm mag}$ at injection is only marginally sensitive to α, insofar as the iron path length increases. Efficiency sensitivity to yoke thickness at injection is negligible. Larger α requires thicker yokes to realize full magnetic efficiency capability.

Figures 1 and 2 are in fact the strawmen dipole and quadrupole configurations, D21b and Q28f (with $\beta = 28°$ and $\alpha = 12°$), respectively.

A.2 DIPOLE-QUADRUPOLE TRACKING

Tracking of magnetic efficiencies for the chosen strawmen designs of the previous section is shown in Table A-3, part 3a. Tracking is initially improved through adjustment of yoke thicknesses w_y and pole taper angles α so as to match $\eta_{\rm mag}$'s at extraction and injection while simultaneously roughly matching the magnitudes and extents of H in the iron according to the prescription for good tracking given by Eq. (19). The dipole α is first increased so as to match dipole and quadrupole extraction efficiencies and to reduce the maximum H in the dipole iron. Then the exact quadrupole current corresponding to the dipole extraction current giving a dipole field of 1.3 T is calculated. Iteratively adjusting yoke thicknesses to match magnetic efficiencies and H's in the iron results in the design of Table A-3, part 3b. Tracking is to within 0.0005 from injection to extraction for the design pair D30ff and Q28h1, exceeding the tracking specification given by Eq. (18). [Note that we use $\eta_{\rm mag}$ rather than $\eta_{\rm opt}$ in this intermediate design stage, since after nulling harmonics in the next section $\eta_{\rm opt}$ approaches the value of $\eta_{\rm mag}$.] Figure A-1, illustrating the amount of losses in the iron for the portion of the path where values of $H \geq H|_{\rm lim}$, shows the extent to which the magnitude and extent of H are matched in the dipole and quadrupole.

It is desirable to bolt the quadrupole tip laminations together so as to increase dimensional stability of pole tips during operation. However, this drives a small portion of the quadrupole into saturation and it was predicted that tracking with the dipole would be adversely affected. Tracking of magnetic efficiencies for a quadrupole lamination featuring a bolt hole and a dipole appropriately tapered to match extraction magnetic efficiencies is shown in Table A-3, part 3c. Surprisingly, tracking is to within 0.0005 from injection to extraction for the design pair D26i and Q28g1, exceeding the tracking specification given by Eq. (18). The excellent tracking in the absence of good matching of H in the dipole and quadrupole iron results from the high magnetic efficiency designs chosen in the previous section. Even when a vastly different and less attractive B-H curve (#4 Appendix B

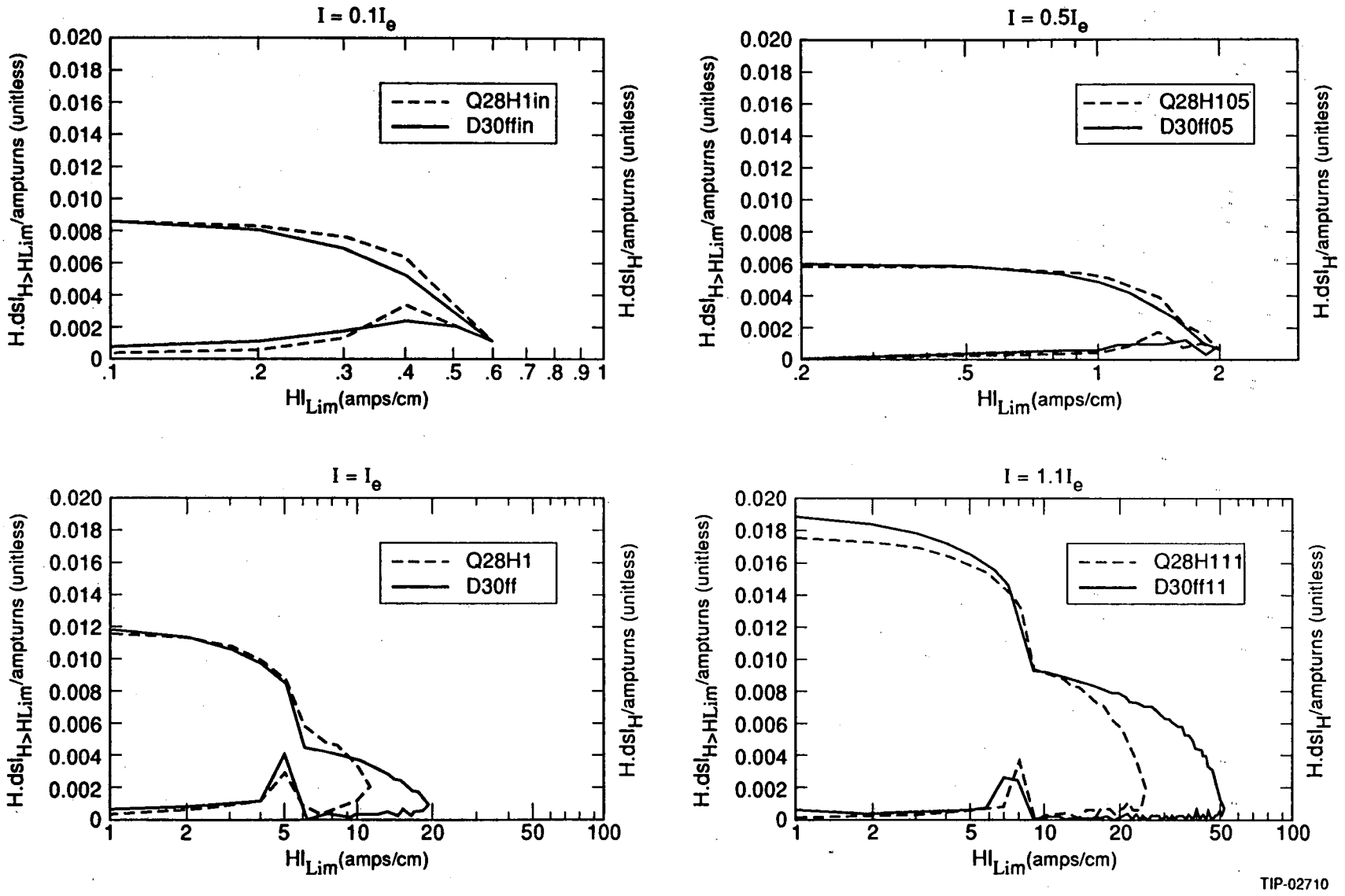

Figure A-1. Total $H \cdot ds$ Losses Along Portion of Path Where $H > H|_{lim}$.

TABLE A-3. Tracking of Strawmen Dipole-Quadrupole Design Pairs.

	Run (#)	α (deg)	w_y (cm)	$\frac{mI_{ext}}{31000}$	$f \equiv I/I_{ext}$ 0.10	0.50	0.80	0.85	0.90	0.95	1.00	1.10
					η_{mag}							
3a	D21b	21.0	10.0	0.975210								0.9805
	Q28f	12.0	5.0	0.967268								0.9861
3b	D30ff	29.9	12.0	0.967011	0.9913	0.9940	0.9923		0.9908		0.9878	0.9807
	Q28h1	12.0	5.4	0.967011	0.9907	0.9934	0.9918		0.9904		0.9877	0.9815
3c	D26i	25.6	10.5	0.971487	0.9909	0.9936	0.9910	0.9900	0.9886	0.9866	0.9833	0.9714
	Q28g1	12.0	5.0	0.971487	0.9904	0.9932	0.9908	0.9898	0.9884	0.9861	0.9826	0.9709
3d	D26i	25.6	10.5	0.971487	0.9820	0.9873	0.9825	0.9807		0.9748	0.9697	0.9526
	Q28g1	12.0	5.0	0.971487	0.9816	0.9871	0.9827	0.9809		0.9746	0.9690	0.9516
All cases use B-H curve #3, except for 6d which uses B-H curve #4 (see Appendix B)												

Figure B-4) is employed, the design pair D26i and Q28g1 track well, as shown in Table A-3, part 3d.

At this point we choose as our strawman pair D26i and Q28g1, which track to within 0.0005. The quadrupole laminations feature a 12.70 mm (1/2 inch) bolt hole.

A.3 MAGNET FIELD QUALITY

The dipole and quadrupole strawman pair pole tips are shimmed using *Mirt*[2,3] so as to null harmonics at injection, where the beam is largest. Harmonics at extraction are subsequently calculated.

Shimmed dipole D26is injection field quality is $|\Delta B/B| \leq 0.0001$ at $|z| \leq 2.5$ cm; extraction field quality is $|\Delta B/B| \leq 0.0014, 0.00080, 0.00040, 0.00016$ at $|z| \leq 2.5, 2.0, 1.5,$ and 1.0 cm, respectively. Thus, while meeting the initial dipole field quality specification at injection, field quality at extraction is over an order of magnitude higher at $z = 2.5$ cm. Optimizing the field quality at extraction roughly switches the injection and extraction results quoted above.

Shimmed quadrupole Q28g1s injection field quality is $|\Delta B/B| \simeq 0.00013$ at $|z| \leq 2.5$ cm; extraction field quality is $|\Delta B/B| \simeq 0.00008$ at $|z| \leq 2.5$ cm. These results greatly exceed the initial quadrupole field quality specification at both injection and extraction.

Finally, tracking performance is checked using the optical efficiencies of the shimmed strawman quadrupole and dipole pair, D26is and Q28g1s. Table A-4 shows that this magnet pair optically tracks to within 0.0011 from injection to extraction.

TABLE A-4. Tracking of Shimmed Strawman Dipole-Quadrupole Design Pair.

Run (#)	α (deg)	w_y (cm)	$\frac{mI_{ext}}{31000}$	$f \equiv I/I_{ext}$ 0.10	0.50	0.80	0.85	0.90	0.95	1.00	1.10
				η_{mag}							
D26is	25.6	10.5	0.971487	0.9908	0.9935	0.9908	0.9897		0.9858	0.9821	0.9694
Q28g1s	12.0	5.0	0.971487	0.9906	0.9934	0.9907	0.9896		0.9851	0.9809	0.9674
				η_{opt}							
D26is	25.6	10.5	0.971487	0.9908	0.9935	0.9907	0.9896		0.9856	0.9818	0.9688
Q28g1s	12.0	5.0	0.971487	0.9911	0.9939	0.9912	0.9900		0.9854	0.9812	0.9676

APPENDIX B
INPUT FILE LISTINGS

Appendix B contains the following *Poisson* input files:

Figure B-1. Automesh input file D26vm2asb.dat for the final dipole design

Figure B-2. Automesh input file Q28g1smra.dat for the final quadrupole design

Figure B-3. Poisson input file for the dipole with with B-H curve #3 (B-H curve of M-27 transformer steel to be used in LEB magnets)

Figure B-4. Poisson input file for the dipole with with B-H curve #4 (alternate B-H curve used to check tracking robustness in Table A-3, part 3d)

Figure B-5. Mirt input file for shimming the dipole

Figure B-6. Mirt input file for shimming the quadrupole.

```
d26vm2asb 7/17/91 720a smoothed near far right corner of bump
$reg nreg=4, dx=0.222, xmax=31.5500,ymax=24.40,npoint=5$
$Po x=0 y=0.$
$Po x=31.5500 y=0.$
$Po x=31.5500 y=24.40$
$Po x=0. y=24.40$
$Po x=0. y=0.$
$reg mat=3, npoint=26$
$Po x=0. y=2.86$
$Po x=1.7000 y= 2.8600$
$po x=3.9 y=2.86$
$Po x=4.15 y= 2.863$
$Po x=4.385 y= 2.892$
$Po x=4.712 y= 2.87$
$Po x=4.928 y= 2.855$
$po x=5.09 y=2.831$
$Po x=5.252 y= 2.799$
$Po x=5.469 y= 2.772$
$Po x=5.684 y= 2.734$
$Po x=5.904 y= 2.718$
$Po x=6.236 y= 2.745$
$Po x=6.458 y= 2.772$
$Po x=6.678 y= 2.823$
$po x=6.836 y=2.862$
$Po x=6.993 y= 2.912$
$po x=7.15 y=2.966$
$Po x=7.305 y= 3.081$
$Po x=12.200 y=13.3$
$Po x=20.4500 y=13.3$
$Po x=20.4500 y=0.$
$Po x=31.5500 y=0.$
$Po x=31.5500 y=24.40$
$Po x=0. y=24.40$
$Po x=0. y=2.86$
$reg mat=1, cur=-31000.0 ,npoint=5$
$Po x=12.6000 y=12.9000$
$Po x=20.0500 y=12.9000$
$Po x=20.0500 y=3.6500$
$Po x=12.6000 y=3.6500$
$Po x=12.6000 y=12.9000$
$reg mat=1, ibound=-1, cur=0., npoint=5$
$Po x=0. y=0.$
$Po x=0. y=2.86$
$Po x=0. y=24.40$
$Po x=31.5500 y=24.40$
$Po x=31.5500 y=0.$
```

Figure B-1. Automesh Input File D26vm2asb.dat for the Final Dipole Design.

```
q28g1smra4 12/12/91 RSmod NI=1.1
$reg nreg=4,dx=0.155,xreg1=19.389,xmax=24.277,
ymax=17.840, npoint=11$
$po x=0. y=0.$
$po x=17.839 y=0.$
$po x=24.277 y=0.$
$po x=24.277 y=3.040$
$po x=24.277 y=6.865$
$po x=17.840 y=17.840 nt=2 r=25.229$
$po x=14.603 y=14.603$
$po x=6.449 y=6.449$
$po x=5.551 y=5.551$
$po x=3.536 y=3.536$
$po x=0. y=0.$
$reg mat=3, npoint=36$
$po x=3.536 y=3.536$
$po nt=3 x=4.8 y=2.604 r=5.0$
$po x=4.865 y=2.57$
$po x=5.0280    y=2.484$
$po x=5.191     y=2.401$
$po x=5.361     y=2.329$
$po x=5.559     y=2.265$
$po x=5.728     y=2.174$
$po x=5.872     y=2.001$
$po x=5.948 y=1.911$
$po x=6.02      y=1.868$
$po x=6.219     y=1.850$
$po x=6.359     y=1.897$
$po x=6.475     y=1.988$
$po x=6.581 y=2.076$
$po x=6.698     y=2.149$
$po x=14.497    y=7.121$
$po x=17.839    y=3.779$
$po x=17.839 y=0.$
$po x=24.277 y=0.$
$po x=24.277 y=3.040$
$po x=23.239    y=3.025$
$po x=23.239    y=6.865$
$po x=22.365    y=7.739$
$po x=21.349    y=7.739$
$po x=21.349    y=8.755$
$po x=17.082    y=13.022$
$po x=16.632    y=13.022$
$po x=16.408    y=12.798$
$po x=14.603    y=14.603$
$po x=6.449 y=6.449$
$po x=6.635 y=6.000$
$po x=6.449 y=5.551$
$po x=6.000 y=5.365$
$po x=5.551 y=5.551$
$po x=3.536 y=3.536$
$reg mat=1 cur=-16591.41 npoint=7$
$po x=9.537 y=2.007$
$po x=14.409 y=6.878$
$po x=17.720 y=3.566$
$po x=16.172 y=2.018$
$po x=14.486 y=3.703$
$po x=11.164 y=0.38$
$po x=9.537 y=2.007$
$reg ibound=-1, npoint=9, cur=0.$
$po x=24.277 y=0.$
$po x=24.277 y=3.040$
$po x=24.277 y=6.865$
$po x=17.840 y=17.840 nt=2 r=25.229$
$po x=14.603 y=14.603$
$po x=6.449 y=6.449$
$po x=5.551 y=5.551$
$po x=3.536 y=3.536$
$po x=0. y=0.$
```

Figure B-2. Automesh Input File Q28g1smra.dat for the Final Quadrupole Design.

```
0
*6 0 *46 6 *8 14000.0 *40 1 1 *31 50 *32 2 *110 8 15 2.50 90.0 2.86  0. *18 1 S
3 0.97 3
1890.       1.
2704.4      1.2
3649.3      1.44
4680.2      1.74
5757.2      2.09
6846.2      2.51
7918.1      3.02
8949.3      3.63
9921.5      4.37
10821.1     5.25
11639.8     6.31
12373.0     7.59
13020.6     9.12
13585.6     10.97
14073.9     13.18
14494.0     15.85
14856.0     19.06
15171.1     22.91
15451.4     27.54
15708.9     33.11
15955.2     39.81
16201.0     47.86
16455.6     57.54
16726.4     69.18
17018.9     83.18
17336.2     100.0
17679.1     120.23
18045.6     144.54
18431.8     173.78
18831.3     208.93
19236.0     251.19
19636.3     301.99
20022.4     363.08
20384.2     436.52
20713.2     524.81
21003.0     630.96
21251.3     758.58
21461.1     912.01
21646.4     1096.48
21869.1     1318.26
22136.6     1584.89
22458.1     1905.46
22844.4     2290.86
23308.7     2754.23
23866.6     3311.3
24537.3     3981.08
25343.4     4786.3
26312.4     5754.39
27477.2     6918.32 S
-1 s
```

Figure B-3. Poisson Input File for the Dipole with B-H Curve #3 (B-H Curve of M-27 Transformer Steel to be Used in LEB Magnets).

```
Feb 27 05:59 1992  copyof568.appen Page 1


0
*6 0 *46 6 *31 50 *32 2 *110 4 16 2.25 90.0 2.86 0.  *18 1 S
3 0.97 3
1890.       2.
2704.4      2.4
3649.3      2.88
4680.2      3.5
5757.2      4.19
6846.2      5.01
7918.1      6.02
8949.3      7.23
9921.5      8.77
10821.1    10.5
11639.8    12.61
12373.0    15.19
13020.6    18.22
13585.6    21.97
14073.9     26.18
14494.0     31.35
14856.0     38.06
15171.1     46.11
15451.4     55.04
15708.9     66.11
15955.2     80.81
16201.0     93.86
16455.6    115.54
16726.4    140.18
17018.9    166.18
17336.2     200.0
17679.1     240.23
18045.6     284.54
18431.8     343.78
18831.3     408.93
19236.0     501.19
19636.3     601.99
20022.4     723.08
20384.2     866.52
20713.2    1044.81
21003.0    1260.96
21251.3    1508.58
21461.1    1812.01
21646.4    2096.48
21869.1    2618.26
22136.6    3084.89
22458.1    3805.46
22844.4    4490.86
23308.7    5454.23
23866.6    6611.3
24537.3    7881.08
25343.4    9486.3
26312.4   10454.39
27477.2   13818.32 S
-1
$EXIT
```

Figure B-4. Poisson Input File for the Dipole with B-H Curve #4 (Alternate B-H Curve Used to Check Tracking Robustness in Table A-3, part 3d).

```
5 S
10 10 S
1.0 R20 1.0 R20 5 R20
3.25 3.2006 3.0540 2.8146 2.4896 2.0891
1.625 1.1116 0.5644 0.0
2.0 1.9696 1.8794 1.7321 1.5321 1.2856 1.00
0.6840 0.3473 0.0
0.0 0.4341 0.855 1.25 1.6070 1.9151 2.1651
2.3492 2.462 2.5
0.0 0.3473 0.6840 1.00 1.2856 1.5321 1.7321
1.8794 1.9696 2.0
17 NPOLE
19 20 21 22 23 24 25 26 26 27 29 30 31 32  33 33 34
16 R8 15 R4 16 16 16 17 17
4 NPAR
2 11 13 15 17  S S
2 9 11 13 15 S S
2 5 7 9 11 S S
2 1 3 5 7 S S
1 NGEN
17 35 13 18 S
0 DUMP
*6 -2 *46 6 *31 50 *110 8 15 2.5 90.0 2.86 0. *18 0
*8 1300.0 *40 1 1 *36 1 S
0 DUMP
*6 0 *46 6 *31 50  *110 8 15 2.50 90.0 2.86  0. *18 1
*8 13000.0 *40 1 1  S
3 0.97 3
1890.       1.
2704.4      1.2
3649.3      1.44
4680.2      1.74
5757.2      2.09
6846.2      2.51
7918.1      3.02
8949.3      3.63
9921.5      4.37
10821.1     5.25
11639.8     6.31
12373.0     7.59
13020.6     9.12
13585.6     10.97
14073.9     13.18
14494.0     15.85
14856.0     19.06
15171.1     22.91
15451.4     27.54
15708.9     33.11
15955.2     39.81
16201.0     47.86
16455.6     57.54
16726.4     69.18
17018.9     83.18
17336.2     100.0
17679.1     120.23
18045.6     144.54
18431.8     173.78
18831.3     208.93
19236.0     251.19
19636.3     301.99
20022.4     363.08
20384.2     436.52
20713.2     524.81
21003.0     630.96
21251.3     758.58
21461.1     912.01
21646.4     1096.48
21869.1     1318.26
22136.6     1584.89
22458.1     1905.46
22844.4     2290.86
23308.7     2754.23
23866.6     3311.3
24537.3     3981.08
25343.4     4786.3
26312.4     5754.39
27477.2     6918.32 S
-1
$EXIT
```

Figure B-5. Mirt Input File for Shimming the Dipole.

```
0 S
13 0                                                                    26312.4    5754.39
1513.8001 R13 1.0 R13 3 R13                                            27477.2    6918.32 S
1.7678 1.8796 1.9834 2.0787 2.165 2.2422 2.3097                        -1
2.3673 2.4148 2.4520 2.4786 2.4946 2.500
1.7678 1.6484 1.5219 1.3889 1.250 1.1057 0.9567
0.8036 0.6740 0.4877 0.3263 0.1635 0.000
11 NPOLE
23 24 25 25 26 27 28 29 30 30 31
15 14 14 13 13 13 12 12 12 11 12
3 NPAR
2 5 7 9 11 S S
2 3 5 7 9  S S
2 1 3 5 7  S S
1 NGEN
22 33 9 18 S
1 DUMP
*6 0 *46 4 *31 50 *32 2 *110 4 16 4.5 45. 2.5 0. *18 1 S
3 0.97 3
1890.       1.
2704.4      1.2
3649.3      1.44
4680.2      1.74
5757.2      2.09
6846.2      2.51
7918.1      3.02
8949.3      3.63
9921.5      4.37
10821.1     5.25
11639.8     6.31
12373.0     7.59
13020.6     9.12
13585.6     10.97
14073.9     13.18
14494.0     15.85
14856.0     19.06
15171.1     22.91
15451.4     27.54
15708.9     33.11
15955.2     39.81
16201.0     47.86
16455.6     57.54
16726.4     69.18
17018.9     83.18
17336.2     100.0
17679.1     120.23
18045.6     144.54
18431.8     173.78
18831.3     208.93
19236.0     251.19
19636.3     301.99
20022.4     363.08
20384.2     436.52
20713.2     524.81
21003.0     630.96
21251.3     758.58
21461.1     912.01
21646.4     1096.48
21869.1     1318.26
22136.6     1584.89
22458.1     1905.46
22844.4     2290.86
23308.7     2754.23
23866.6     3311.3
24537.3     3981.08
25343.4     4786.3
```

Figure B-6. Mirt Input File for Shimming the Quadrupole.

Superconducting Super Collider Laboratory is an equal opportunity employer.